Thieme

MRI Sequences in Head & Neck Radiology – State of the Art

MRI-Sequenzen in der Kopf-Hals-Radiologie – State of the Art

Authors
Gerlig Widmann, Benjamin Henninger, Christian Kremser, Werner Jaschke

Affiliation
Department of Radiology, Medical University of Innsbruck, Austria

Key words
head/neck, MR imaging, MR angiography, MR diffusion/perfusion

received 10.10.2016
accepted 25.01.2017

Bibliography
DOI http://dx.doi.org/10.1055/s-0043-103280
Published online: 2017 | Fortschr Röntgenstr 2017; 189: 413–422 © Georg Thieme Verlag KG Stuttgart · New York
ISSN 1438-9029

Correspondence
Priv.-Doz. Dr. Gerlig Widmann
Department of Radiology, Medical University of Innsbruck
Anichstr. 35
6020 Innsbruck
Austria
Tel.: ++ 43/5 12/50 48 09 27
Fax: ++ 43/5 12/50 46 78 09 27
Gerlig.Widmann@i-med.ac.at

ZUSAMMENFASSUNG

Hintergrund Magnetic resonance imaging (MRI) ist ein essentielles bildgebendes Verfahren für die Beurteilung von Kopf-Hals Erkrankungen. Die diagnostische Aussagekraft der MRI ist jedoch stark von der entsprechenden Auswahl und Interpretation der Protokolle und Sequenzen abhängig. Das Ziel dieses Beitrags ist es, State-of-the-art-Sequenzen für die klinische Routine der Kopf-Hals-MRI zusammenzufassen und die Evidenz zu beschreiben, für welche medizinische Fragestellungen diese Sequenzen nützlich sind.

Methode Literaturübersicht von State-of-the-art-Sequences in der Kopf-Hals-MRI.

Ergebnisse und Schlussfolgerung Basis-Sequenzen (T1w, T2w, T1wC+) und Fett-Suppressionstechniken (TIRM/STIR, Dixon, Spectral Fat sat) sind wichtige Bestandteile des diagnostischen Workup von Entzündungen, kongenitalen Läsionen und Tumoren inclusive Staging. Zusätzliche Sequenzen (SSFP (CISS, FIESTA), SPACE, VISTA, 3D-FLAIR) werden verwendet für Pathologien der Hirnnerven, des Labyrinths und zur Beurteilung des endolymphatischen Hydrops bei Menière's Erkrankung. Gefäß- und Perfusionssequenzen (3D-TOF, TWIST/TRICKS angiography, DCE) kommen bei vaskulären Kontaktsyndrom, Gefäßmalformationen und zur Analyse von mikrovaskulären Parametern der Gewebsperfusion zum Einsatz. Diffusionsgewichtete Bildgebung (EPI-DWI, non-EPI-DWI, RESOLVE) ist hilfreich beim Cholesteatom, Abschätzung von Malignität und der Beurteilung des Behandlungsansprechens und Remissionsstatus bei Kopf-Hals-Malignomen. Das Verständnis der MRI-Sequenzen und die enge Zusammenarbeit mit den zuweisenden Klinikern verbessert die diagnostische Aussagekraft der MR-Bildgebung in der täglichen Routine und ist wegweisend für die weitere Forschung in dieser faszinierenden bildgebenden Modalität.

Kernaussagen:
- Das Verständnis von MRI-Sequenzen ist für die korrekte und verlässliche Interpretation von MRI-Befunden essentiell.
- MRI Protokolle müssen sorgfältig anhand relevanter klinischer Informationen ausgewählt werden.
- Die enge Zusammenarbeit mit den zuweisenden Klinikern verbessert die Ausschöpfung der diagnostischen Möglichkeiten der MR-Bildgebung.

ABSTRACT

Background Magnetic resonance imaging (MRI) has become an essential imaging modality for the evaluation of head & neck pathologies. However, the diagnostic power of MRI is strongly related to the appropriate selection and interpretation of imaging protocols and sequences. The aim of this article is to review state-of-the-art sequences for the clinical routine in head & neck MRI and to describe the evidence for which medical question these sequences and techniques are useful.

Method Literature review of state-of-the-art sequences in head & neck MRI.

Results and Conclusion Basic sequences (T1w, T2w, T1wC+) and fat suppression techniques (TIRM/STIR, Dixon, Spectral Fat sat) are important tools in the diagnostic workup of inflammation, congenital lesions and tumors including staging. Additional sequences (SSFP (CISS, FIESTA), SPACE, VISTA, 3D-FLAIR) are used for pathologies of the cranial nerves, labyrinth and evaluation of endolymphatic hydrops in Menière's disease. Vessel and perfusion sequences (3D-TOF, TWIST/TRICKS angiography, DCE) are used in vascular contact syndromes, vascular malformations and analysis of microvascular parameters of tissue perfusion. Diffusion-weighted imaging (EPI-

This document was downloaded for personal use only. Unauthorized distribution is strictly prohibited.

DWI, non-EPI-DWI, RESOLVE) is helpful in cholesteatoma imaging, estimation of malignancy, and evaluation of treatment response and posttreatment recurrence in head & neck cancer. Understanding of MRI sequences and close collaboration with referring physicians improves the diagnostic confidence of MRI in the daily routine and drives further research in this fascinating image modality.

Key Points:

- Understanding of MRI sequences is essential for the correct and reliable interpretation of MRI findings.
- MRI protocols have to be carefully selected based on relevant clinical information.
- Close collaboration with referring physicians improves the output obtained from the diagnostic possibilities of MRI.

Citation Format

- Widmann G, Henninger B, Kremser C et al. MRI Sequences in Head & Neck Radiology – State of the Art. Fortschr Röntgenstr 2017; 189: 413–422

Introduction

Over the last decade, magnetic resonance imaging (MRI) has become an essential imaging modality for the evaluation of head & neck pathology. The ongoing improvement in MRI technology including 1.5 and 3.0 Tesla (T) scanners, multi-channel coils, refined image data acquisition, and sequence development has continuously increased the quality and diagnostic power of MR images.

MRI produces images with unparalleled tissue contrast and is able to obtain tissue characteristics in different sequences without the burden of radiation. It allows for a profound evaluation of the complex head & neck anatomy and identification of a large variety of inherited, infectious and tumorous lesions. Assessment of infiltration depth and the topographic relationship of tumor to critical vascular structures or anatomic spaces deliver essential information for surgical treatment options. MRI allows for evaluation of cranial nerves, the labyrinth and intracranial structures. With the application of contrast-enhanced sequences, tissue perfusion, vessel analysis and dynamic angiographic imaging are obtained. The characterization of head & neck lesions ranges from cystic to solid and clearly benign to definitely malignant. Estimation of malignancy is critical in lymph node imaging and for the evaluation of treatment response. Diffusion-weighted and dynamic contrast-enhanced techniques are promising tools providing biomarkers to guide treatment in head & neck cancer.

The aim of the present paper is to review state-of-the-art sequences in head & neck MRI. The goal is to demonstrate why and for which medical question these sequences and techniques are useful. The authors do not claim to cover all available sequences and limit technical descriptions to basic understanding.

MRI sequences – main pathologies/ field of application – diagnostic clues

In this review MRI sequences were grouped as follows: Basic sequences (T1w, T2w, T1wC+), fat suppression techniques (TIRM/STIR, Dixon, spectral fat sat), additional sequences (SSFP (CISS, FIESTA), SPACE, VISTA, 3D-FLAIR), vessel and perfusion sequences (3D-TOF, TWIST/TRICKS angiography, DCE), and diffusion-weighted imaging sequences (EPI-DWI, non-EPI-DWI, RESOLVE). For each group of sequences, the field of application is described and the main pathologies and diagnostic clues are reviewed. A summary can be found in ▶ **Table 1**. For demonstration purposes of the diagnostic power of MRI, three clinical cases are shown in ▶ **Fig. 1 – 3**.

Basic sequences: T1w, T2w, T1wC+

MRI produces an image by recording the signal generated from water protons in tissue after the application of a resonant electromagnetic radiofrequency field. The basic sequences include measurements with different spin-echo (SE), turbo- or fast spin-echo (TSE/FSE), and gradient-echo (GE) sequences. Contrast in the obtained images is influenced by several tissue parameters such as proton density, T1 and T2 relaxation times, flow velocity in blood vessels, susceptibility and others [1]. Fluid and mucus appear with a low T1-weighted (w) and high T2w signal, and tumors as isointense or hypointense on both T1w and T2w images. Fat shows a high T1w and T2w signal intensity. Application of a paramagnetic gadolinium-based contrast medium shortens T1 relaxation times resulting in a signal increase in T1w contrast-enhanced (C+) images. Compared with the standard field strength of 1.5 T, 3 T MRI has the advantage of increased signal-to-noise ratio and higher resolution. However, these advantages may be outweighed by an increase in artifacts due to motion, susceptibility and B1 inhomogeneities. Last generation scanners and dedicated circular polarized multichannel head/neck coil technology have increased image quality.

The high T1w and T2w soft tissue discrimination together with T1wC+ sequences are extremely useful in the diagnostic workup of inflammation and cancer. Inflammation usually shows diffuse swelling and edema with an increase in the T2w signal and contrast enhancement on T1wC+ [2]. It may range from local infection such as in tonsillitis to diffuse inflammatory phlegmon spread. In contrast, an abscess is classified as a circumscribed T1wC+ hypointense, non-enhancing mass with a T1wC+ highly intense contrast-enhancing wall. These features are important in the diagnosis of deep neck abscesses such as in the retropharyngeal space [3]. Congenital lesions such as thyreoglossal duct remnants and anomalies of the branchial arches typically presenting as cysts, sinus tracts, fistulae or cartilaginous remnants may be diagnosed based on location, clinical symptoms and MRI findings [4]. Lesions of the salivary glands or stone-related pathologies can be clearly depicted. Teeth fillings like amalgam or gold or dense

This document was downloaded for personal use only. Unauthorized distribution is strictly prohibited.

▶ **Table 1** Summary of suitable MRI sequences, main pathologies/field of application, and diagnostic clues.

▶ **Tab. 1** Zusammenfassung nützlicher MRI Sequenzen, Hauptpathologien / Anwendungsfeld und diagnostische Merkmale.

MRI sequences	main pathologies/field of application	diagnostic clues
T1w, T2w, T1wC+	inflammation	high signal on T2w and T1wC+, swelling, preserved mucosal lining [2]
	abscess	circumscribed T1wC+ hypointense non-enhancing mass with a T1wC+ highly intense contrast-enhancing wall [3]
	congenital lesions (thyreoglossal duct remnants and anomalies of the branchial arches)	cysts, sinus tracts, fistulae or cartilaginous remnants based on location and clinical symptoms [4]
	sinonasal inverted papilloma	convoluted cerebriform pattern on T2w and T1wC+ [6]
	paraganglioma	"salt and pepper" appearance (30 – 40 %) [7]
	cancer	intermediate to high signal in T2w, high signal in T1wC+, mass, infiltration, inhomogeneity, necrosis
	perineural invasion	T2w and T1w thickening and T1wC+ contrast enhancement along the cranial nerve [8]
	dural invasion	nodular dural enhancement on T1wC+ and width of enhancement of more than 5 mm [9]
	mandibular bone invasion	replacement of peripheral hypointense signal (cortical bone) through either tumor signal intensity on both T1w and T2w, or central hyperintense signal (medullary bone) is replaced by intermediate tumor signal [11]
	neoplastic invasion of laryngeal cartilages	low T1w signal, similar to that of tumor T2w signal and similar to tumor T1wC+ signal [12]
	residual cancer after chemoradiation therapy	intermediate T2 signal intensity similar to that of the untreated tumor with areas formed a focal expansible mass > = 1 cm [14]
	dissection	high T1w signal in the vessel wall [15]
TIRM/STIR, Dixon, spectral fat sat	edema, swelling, tumor	high signal in TIRM/STIR
	necrosis, cystic lesions	high signal in TIRM/STIR
	adipose tissue (lipoma, cholesterol granuloma)	suppressed signal
	lymph node metastasis	nodal size (minimum axial diameter of 8 – 9 mm in level II and 7 – 8 mm for the rest of the neck), loss of hilar structure and necrosis (varying level of low-to-high signal intensity on T2w fat sat depending on keratinization, and coagulation and liquefaction necrosis) [18]; lower signal than regular or reactive lymph nodes on inverted TIRM/STIR [16]
	extranodal tumor spread	nodal size, shaggy margin and flare sign on T2w fat sat [19]
SSFP (CISS, FIESTA), SPACE, VISTA, 3D-FLAIR	cerebellopontine angles and inner ear (facial and vestibulocochlear nerves, schwannomas)	high-resolution dark signal of cranial nerves and very high signal of liquor in SSFP [20]
	labyrinthitis	lower signal intensity than liquor on SSFP [22]
	menière's disease	endolymphatic hydrops as ratio of high post-gadolinium 3D-FLAIR signal intensity in the perilymphatic space and the high signal in MRI cisternographic sequences in both endolymph and perilymph: vestibule (mild: 34 – 50 %, significant: > 50) cochlea (mild: extrusion of the scala media, significant: scala media larger than scala vestibuli) [25]
3D-TOF, TWIST/ TRICKS angiography, DCE	vascular contact syndromes	point, longitudinal and loop compression as well as indentation of cranial nerves on 3D-TOF [26]
	infantile hemangioma	arterial enhancement on TWIST with gadofosveset trisodium [30]
	venous malformation	venous enhancement on TWIST with gadofosveset trisodium [30]
	lymphatic malformation	no enhancement on TWIST with gadofosveset trisodium [30]
	arteriovenous malformation	arterial and venous enhancement on TWIST with gadofosveset trisodium [30]
	hypoxia	low K^{trans} [32]

This document was downloaded for personal use only. Unauthorized distribution is strictly prohibited.

▶ **Table 1** (Continuation)

MRI sequences	main pathologies/field of application	diagnostic clues
	paraganglioma	high peak enhancement, SER, and short TME on DCE [37]
	schwannoma	low peak enhancement and SER with a longer TME on DCE [37]
diffusion-weighted imaging	primary tumors	low ADC values (lymphoma, followed by carcinoma, benign tumor and cystic lesions) [47]
	lymph node staging	low ADC values [49]
	residual cancer after chemoradiation therapy	lower increase in the percentage change of the mean ADC or decrease in ADC during treatment [51, 52]
	cholesteatoma	high signal on DWI [60]
	Granulation tissue, fibrous tissue, cholesterol granuloma or serous fluid	Low signal on DWI [65]

bone do not cause severe artifacts (as typically seen in computed tomography CT), which makes MRI a superior image modality for delineating tumors in the oropharynx and oral cavity [5]. The ability to discriminate fluid and mucus from soft tissue is extremely helpful in the imaging of sinonasal tumors. The convoluted cerebriform pattern on T2w and T1wC+images is a reliable feature of sinonasal inverted papilloma, with focal loss of the cerebriform pattern to be a clue to the diagnosis of focal malignancy [6]. Paraganglioma may show the typical "salt and pepper" appearance in about 30 – 40 % of cases [7]. Skull base pathologies including various complications from sinonasal and mastoid infections such as orbital cellulitis, orbital abscess, meningitis, epidural and intracranial abscess or thrombosis of venous sinuses are typical MRI indications. Perineural tumor invasion may be diagnosed by the thickening and contrast enhancement of cranial nerves including the presence of skip lesions and dural invasion is best indicated by nodular dural enhancement and a width of enhancement of more than 5 mm [8, 9]. The correct staging of head & neck tumors is the basis for recommendations regarding resectability (T4b vs. T4a, surgery vs. radiation therapy), extent of resection (enoral laser vs. transcervical), lymph node dissection (selective vs. modified radical), and many more [10]. Mandibular bone invasion may be indicated when signs of peripheral hypointense signal (cortical bone) are replaced by either tumor signal intensity on both T1w and T2w images, or by the replacement of the central hyperintense signal (medullary bone) with an intermediate tumor signal [11]. Limiting factors are larger slice distance, periapical and periodontal disease, and remodeling after trauma or tooth extraction. For the detection of neoplastic invasion of laryngeal cartilages, the criteria of low T1w signal, similar to that of tumor T2w signal and similar to tumor T1wC+ signal indicate cartilaginous invasion by a tumor, whereas the criteria of low T1w signal, higher than tumor T2w signal and greater than tumor T1wC+ signal indicate cartilaginous inflammation with both very high PPVs and NPVs [12]. Both malignant and benign post-treatment masses show contrast enhancement making a clear statement regarding treatment response and recurrences difficult [13]. Early post-treatment T2w images after chemoradiation therapy show low T2 signal intensity with a flat-edged or retracted margin in lesions with local control, whereas an intermediate T2 signal intensity, similar to that of the untreated tumor with areas forming a focal expansible mass > = 1 cm is highly predictive of residual cancer [14]. Dissection of the carotid artery may rarely lead to oculomotor paresis or paresis of the distal cranial nerves IX, X, XI, XII (Collet-Siccard-Syndrome) and may be diagnosed by increased T1w signal within the vessel wall [15].

Fat suppression: TIRM/STIR, Dixon, spectral fat sat

In head & neck radiology fat suppression usually involves spectral or frequency selective fat suppression, T1-based short tau inversion recovery (STIR) techniques such as fast spin echo-based turbo inversion recovery magnitude (TIRM), chemical shift-based Dixon methods, and hybrid techniques combining several of these fat suppression techniques such as SPIR (spectral presaturation with inversion recovery). STIR/TIRM sequences must not be acquired after contrast agent injection, as in this case the contrast agent uptaking mass can be nulled in signal due to the shortening of T1 time by the contrast agent. This also applies for T2w STIR/TIRM sequences, as the fat suppression is based on the T1 time of the tissue in all inversion recovery sequences. T2w TIRM provides fast image acquisition with homogeneous and global fat suppression giving high signal intensity for water-containing structures. It is a useful sequence for the overview of edema, swelling, and necrosis and cystic lesions such as in infection or malignancy. Using a contrast-inverted display of TIRM/STIR images, a darker signal than regular or reactive lymph nodes (LN) may increase the sensitivity and specificity of pathologic LN detection [16].

In Dixon methods both in-phase and opposed-phase images are acquired simultaneously which can be combined mathematically to fat only and water only images. The Dixon method can be applied to both T1w and T2w sequences [17]. The advantages of suppressing the signal from fat is to suppress artifacts due to high fat signals, to improve T2 contrast between fatty and non-fatty tissue, to enable detection of enhancing tumors hidden in fatty tissue, and the proof of adipose tissue, such as in lipoma, or cholesterol granuloma. Reading T1w and T2w basic sequences and T2w fat sat images is important because the very high STIR/TIRM

This document was downloaded for personal use only. Unauthorized distribution is strictly prohibited.

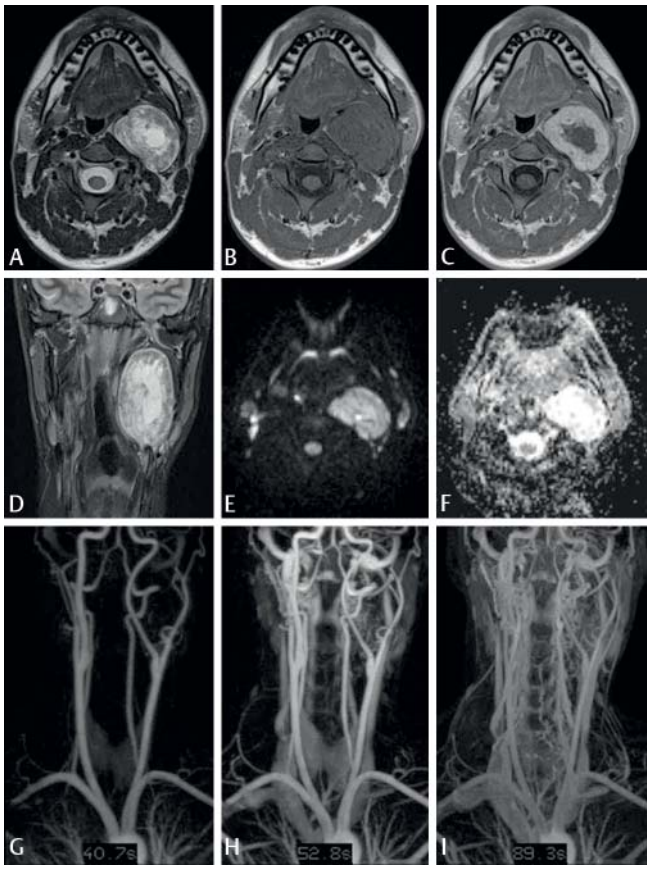

▶ **Fig. 1** Case 1: 30-year-old man presenting with indolent swelling of the left neck for more than 1 year and without complaints. Basic sequences **A**–**C**: Ovoid shaped lesion in the left carotid space with clear margins. No signs of infiltration of surrounding tissues. **A** T2w shows a mixed very high and inhomogeneous high signal intensity indicating areas of necrosis. **B** T1w shows isointense signal intensity. **C** T1wC+ shows marked peripheral enhancement with central non-enhancing necrotic area. Fat suppression sequence **D**: TIRM shows similar signal intensity as T2w with no evidence of fat content or perilesional edema. Diffusion-weighted imaging **E**–**F**: High signal intensity on DWI and ADC map, indicating no diffusion restriction and thus no typical sign of malignancy. Vessel sequences **G**–**F**: TWIST angiography after 40.7 s, 52.8 s, and 89.3 s show no arterial enhancement, which is not typical for a paraganglioma. MRI diagnosis: schwannoma (histo-pathologically confirmed).

▶ **Abb. 1** Fall 1: 30 Jahre alten Mannes mit einer indolenten Schwellung der linken Halsseite welche seit mehr als einem Jahr besteht und keine Beschwerden verursacht. Basis Sequenzen **A**–**C**: Ovaloide Läsion im linken Karotisraum mit klarer Begrenzung. Keine Zeichen einer Infiltration von umgebenden Gewebe. **A** T2w zeigt gemischt sehr hohe und inhomogen hohe Signalintensität, hinweisend auf Nekrosezonen. **B** T1w zeigt isointense Signalintensität. **C** T1wC+ zeigt deutliche periphere Kontrastmittelaufnahme mit zentralen nichtanreichernden nekrotischen Arealen. Fett-Suppresions-Sequenz **D**: TIRM zeigt ähnliche Signalintensität wie in T2w ohne Evidenz auf fettigen Inhalt oder periläsionales Ödem. Diffusionsgewichtete Bildgebung **E**–**F**: Hohe Signalintensität in der DWI und ADC map und somit keine Diffusionsrestriktion und kein typisches Zeichen für Malignität. Gefäßsequenzen **G**–**F**: TWIST Angiographie nach 40,7 s, 52,8 s, und 89,3 s zeigt kein arterielles Enhancement, was untypisch für ein Parqaganglіom ist. MRI Diagnose: Schwannom (histopathologisch bestätigt).

signal and T1wC+ contrast enhancement related to reactive inflammation may lead to overestimation of the size of the real tumor mass and potential overestimation of the T stage [12]. In T2w fat sat images, lymph node metastasis may show an enlarged size (minimum axial diameter of 8 – 9 mm in level II and 7 – 8 mm for the rest of the neck), loss of hilar structure and necrosis (varying level of low-to-high signal intensity depending on keratinization, and coagulation and liquefaction necrosis) [18]. Extranodal tumor spread may be indicated by the criteria of nodal size, shaggy margin (obliterated fat spaces between the metastatic LN and adjacent tissues), and flare sign (high-intensity signals in the interstitial tissues around and extending from a metastatic LN) [19].

Additional sequences: SSFP (CISS, FIESTA), SPACE, VISTA, 3D-FLAIR

Steady-state free precession (SSFP) sequences such as constructive interference steady state (CISS) and fast imaging employing steady-state acquisition (FIESTA or trueFISP) are a group of GE sequences in which a steady state develops between pulse repetitions for both the longitudinal and transverse relaxation values. These sequences provide a high signal in tissues with high T2 / T1 ratios, such as cerebrospinal fluid and fat, and enable submillimeter spatial resolution allowing isotropic 3 D acquisitions which can be used for multiplanar reconstructions. This makes SSFP a mainstay in the evaluation of the cerebellopontine angles and inner ear, allowing for a precise differentiation between branches of the facial and vestibulocochlear nerves. SSFP has become essential in identifying the vestibular cochlear nerves before cochlear implant surgery. It allows for the accurate detection of small masses such as schwannomas in the cerebellopontine angles and internal auditory canals, and detailed evaluation of the labyrinth of the inner ear [20, 21]. In addition to a high signal in T1wC+, labyrinthitis may show a lower signal than fluid on SSFP [22]. 3 D imaging can be further obtained using special fast spin echo techniques, such as sampling perfection with application-optimized contrasts using different flip angle evolutions (SPACE) or volumetric isotropic turbo spin echo acquisition (VISTA).

3 D fluid-attenuated inversion recovery (3D-FLAIR) sequences produce high-resolution 3 D images with a suppressed fluid signal. 3D-FLAIR allows separate visualization of endo-and perilymphatic components and has become a new diagnostic tool for the visualization of endolymphatic hydrops in Menière's disease [23]. Gadolinium chelate-enhanced images are typically obtained 24 h after microscopically controlled intratympanic application (i.t) (8-times diluted), or 4 h after intravenous (i. v.) application [24]. The gadolinium chelate enters the inner ear via the round and oval windows (i. t.) or via the blood-labyrinth barrier (i. v.) and leads to a high signal intensity only in the perilymphatic space. In contrast, T2w SPACE and other MR cisternographic sequences show a bright signal in both the endolymph and perilymph. As the normal limit of the ratio of the endolymphatic over the vestibular area is 33 %, a new image-based classification of endolymphatic hydrops has been proposed for both the vestibule (mild: 34 – 50 %, significant: > 50) and the cochlea (mild: extrusion of the scala media, significant: scala media larger than scala vestibuli) [25].

This document was downloaded for personal use only. Unauthorized distribution is strictly prohibited.

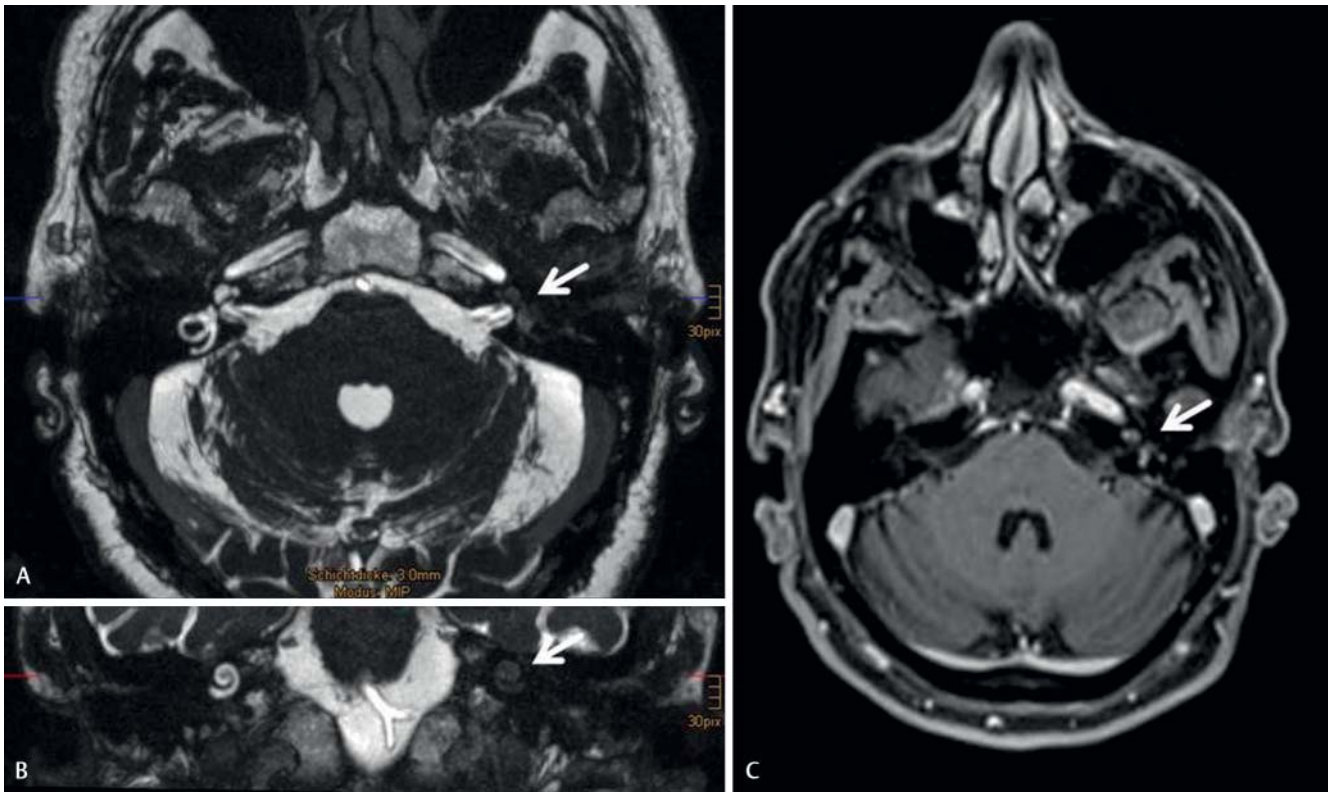

▶ **Fig. 2** Case 2: 75-year-old man with acute hypacusis, nausea and pain in the left ear. **A–B** CISS 3 D MIP reconstruction in axial and coronal plane shows loss of fluid signal in the left cochlea and vestibulum (arrow). **C** T1wC+ shows contrast enhancement of the left cochlea and vestibulum. MRI diagnosis: labyrinthitis.

▶ **Abb. 2** Fall 2: 75 Jahre alter Mann mit akuter Hypoacusis, Nausea und Schmerzen im linken Ohr. **A–B** CISS 3 D MIP Rekonstruktion in axialer und koronaler Ebene zeigt eine deutliche Flüssigkeitssignalminderung in der linken Chochlea und Vestibulum (Pfeil). **C** T1wC+ zeigt eine Kontrastmittelaufnahme der linken Chochlea und Vestibulum (Pfeil). MRI Diagnose: Labyrinthitis.

Vessels and perfusion: 3D-TOF, TWIST/TRICKS angiography, DCE

3 D time-of-flight (3D-TOF) angiography is a contrast-free method which provides high-resolution visualization of small vessels. It is based on GE sequences with a short TR using the phenomenon of inflow-related enhancement of spins to obtain a difference between the unsaturated and presaturated spins in order to create a bright vascular image. Vessels in the cerebellopontine angle from the circle of Willis can be clearly detected and in combination with SSFP images, vascular contact syndromes related to point, longitudinal and loop compression as well as indentation of cranial nerves can be reliably diagnosed [26].

Time-resolved angiography with interleaved stochastic trajectories (TWIST) or time-resolved imaging of contrast kinetics (TRICS) MR angiography is a technique which provides high temporal resolution images during the arterial, capillary and venous phases [27]. This technique is a reliable tool for the evaluation of the feeding arteries, the nidus and draining veins of arteriovenous malformations of the head & neck [28, 29]. Combined with basic sequences, TWIST using the blood pool contrast agent gadofosveset trisodium may achieve the highest accuracy with complete anatomical characterization of infantile hemangioma and lymphatic and venous malformation [30]. Based on the timing of enhancement, infantile hemangioma shows arterial, venous malformation, venous, lymphatic malformation, none and arteriovenous malformation, arterial and venous enhancement [30].

Dynamic contrast-enhanced (DCE) MRI is a complex technique for the analysis of microvascular parameters of tissue perfusion [31, 32]. It requires the placement of a region of interest within the tumor to calculate time-intensity curves (TIC) and semiquantitative parameters such as the area under the curve (AUC, relative quantity of contrast over time), peak enhancement (maximum concentration of contrast), wash-in (velocity of enhancement), wash-out (velocity of enhancement loss), maximum signal enhancement ratio (SER), and time to maximum enhancement (TME). Furthermore, pharmacokinetic modelling is used to obtain quantitative parameters such as K^{trans} (volume transfer coefficient between plasma and extravascular extracellular space), k_{ep} (rate constant between plasma and extravascular extracellular space), V_b (blood volume), V_p (plasma volume), and others. Today, DCE MRI is still considered subjective and time-consuming and is not a completely standardized technique for the evaluation of anti-vascular therapies. The output may vary between and within institutions, because of differences in T1 analysis, methods to measure arterial input function (AIF), choice of ROI, scanner model, pharmacokinetic model and time point chosen during

This document was downloaded for personal use only. Unauthorized distribution is strictly prohibited.

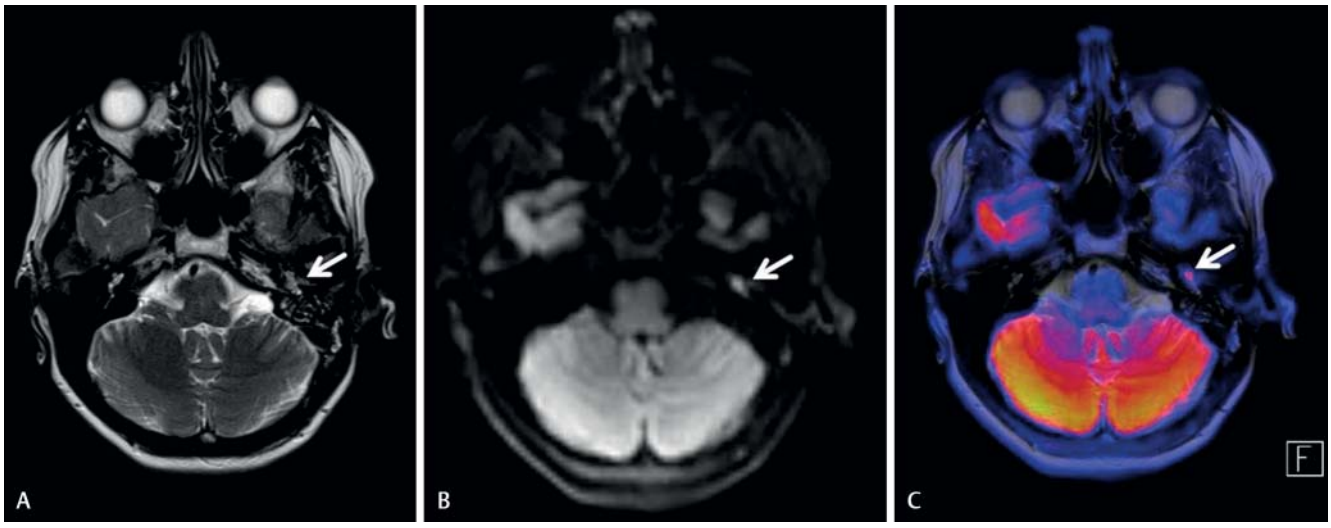

▶ **Fig. 3** Case 3: 41-year-old female with suspicion of cholesteatoma. **A** T2w shows a slightly hyperintense nonspecific lesion/opacification in the tympanic cavity of the left side (arrow). **B** EPI-DWI RESOLVE shows a small hyperintense correlate (arrow). **C** Fused images better depict the anatomic correlation. MRI diagnosis: Cholesteatoma (histo-pathologically confirmed).

▶ **Abb. 3** Fall 3: 41 Jahre alte Frau mit V. a. Cholesteatom. **A** T2w zeigt eine gering hyperintense unspezifische Läsion/Verschattung im linken Cavum tympani (Pfeil). **B** EPI-DWI RESOLVE zeigt ein kleines hyperintenses Korrelat (Pfeil). **C** Fusionierte Bilder erleichtern die anatomische Zuordnung. MRI Diagnose: Cholesteatom (histopathologisch bestätigt).

treatment [33]. However, K^{trans} emerged as a marker for tumor hypoxia indicating poorer survival or poorer treatment response and has the potential to be a useful biomarker to guide treatment in head & neck squamous cell cancer [32, 34, 35]. It may also have the potential to identify early locoregional recurrence and differentiate metastatic lymph nodes from normal nodes [36]. DCE MRI may differentiate paraganglioma with high peak enhancement, SER, and short TME from schwannoma which shows a relatively low peak enhancement and SER with a longer TME [37].

Diffusion-weighted imaging (EPI-DWI, non-EPI-DWI, RESOLVE)

Diffusion-weighted imaging (DWI) reflects the microanatomy of tissues based on the molecular diffusion of protons corresponding to the Brownian motion. Image acquisition is based on dephasing and rephrasing of protons by applying pairs of opposing magnetic field gradients along a certain diffusion direction. The obtained apparent diffusion co-efficient (ADC) estimates the mobility of protons moving within tissue which is limited in dense hypercellular tissues such as tumor and increased in edema, inflammation and fibrosis with low cellularity [38]. Low b-values (different sensitizing effects of the gradient ranging from 0 up to 2000 s/mm²) reflect microvascularity and perfusion of tissues while higher b-values of 800 or 1000 s/mm² demonstrate cellular-based changes in tissue diffusivity. Mean pretreatment and posttreatment ADC values are typically calculated by delineation of total tumor volume on DWI MRI. DWI has become an essential complementary sequence to standard MRI sequences.

A variety of different DWI techniques are used, which basically can be divided into echo-planar imaging (EPI)-based and non-EPI-based techniques. Single-shot (SS) EPI-DWI can be seen as a widely available standard DWI technique. It is relatively insensitive to motion but prone to susceptibility artifacts, chemical shift and geometric distortion, has a limited spatial resolution and relatively thick sections [39]. Standard DWI may be significantly limited by artifacts from the skull base [40]. TSE-based DWI is a spin-echo-based SS or multi-shot (MS) technique with longer echo time and a higher signal-to-noise ratio than SS EPI-DWI. However, these sequences don't show the susceptibility artifacts that are observed with standard EPI-DWI and better spatial resolution in the middle ear is possible [22]. Furthermore, thinner slices can be obtained than with EPI sequences. The SS version of TSE-DWI is a diffusion-weighted HASTE sequence with excellent motion insensitivity and less sensitivity to susceptibility artifacts and geometric distortion than the EPI sequence [41, 42]. A non-EPI DWI sequence with periodically rotated overlapping parallel lines with enhanced reconstruction (PROPELLER or BLADE) has been reported as useful in avoiding geometric distortion. The k-space data are acquired in the form of rotating sections (blades). The resulting oversampling of the central k-space leads to an improved signal-to-noise ratio (SNR) and to the reduction of motion and susceptibility artifacts [41, 43, 44]. RESOLVE DWI is a new approach for obtaining DWI images with high quality, delivering sharp images at high spatial resolution and reduced slice thickness. It uses the same diffusion preparation as SS EPI. By dividing the k-space trajectory into multiple segments in the phase encoding direction, the echo time (TE) can be reduced to increase the quality of the acquired images. Furthermore, RESOLVE DWI is largely free of distortion, susceptibility and T2* blurring artifacts. Slice thickness for the DWI (and its corresponding anatomical T1w or T2w) should not exceed 3 mm.

In head & neck cancer DWI is used for the characterization of primary tumors and nodal metastases, the prediction and monitoring of treatment response after chemo and/or radiation ther-

This document was downloaded for personal use only. Unauthorized distribution is strictly prohibited.

apy, and the differentiation of post-therapeutic radiation changes and residual or recurrent disease [45]. Regarding primary tumors, it has been clearly demonstrated that malignant lymphoma has the lowest ADC values followed by carcinoma, benign tumor, and cystic lesions, and that ADC values significantly differ between well-differentiated and poorly differentiated lesions [46, 47]. ADC significantly correlates with cellularity, stromal component, and nuclear-cytoplasmic ratio; and the positive correlation of ADC and stromal component may partly reflect the poor prognostic value of high pre-treatment ADC [48].

For lymph node staging ADC values have found to be the strongest independent predictor for the presence of nodal metastases [49] and significantly improve the detection of small metastatic lymph nodes (4 – 9 mm), which remain false-negative based on pure size and morphology criteria [50]. For the evaluation of treatment response it has been shown that two-week intra-treatment ADCs are predictors of outcome, as a lower increase in the percentage change of the mean ADC, higher skewness, and higher kurtosis are significantly more likely to show local failure than local control [51]. A decrease in ADC during treatment is strongly indicative of a time point of tumor resistance and treatment failure [52]. DWI seems even superior to FDG PET/CT for post-treatment recurrence [53].

Unfortunately, ADC values may be affected by the selected technique and MR imaging system due to differences in gradient systems, coils, pulse-sequence design, imaging parameters, and artifacts related to susceptibility effects or eddy currents [54]. As a consequence, ADC thresholds defined in the literature cannot be easily extrapolated and each center will need to obtain site-specific values [55, 56].

Cholesteatoma appears hyperintense on DWI obtained with b-factors of 800 or 1000 sec/mm^2; this is similar to a histologically identical lesion, the epidermoid cyst [57]. Granulation tissue, fibrous tissue, cholesterol granuloma or serous fluid has a low signal intensity on DWI (at a b-factor of 800 sec/mm^2). Visual comparison of DWI images obtained with a b-factor of 800 sec/mm^2 without calculation of the apparent diffusion coefficient is sufficient for diagnostic analysis [58, 59]. The reason for the high signal intensity is assumed to be a T2 shine-through effect or the restricted molecular diffusion of cholesteatoma. SS EPI-DWI frequently leads to artifacts, which could mask areas of restricted diffusion in a cholesteatoma and therefore SS EPI-DWI is no longer recommended [60, 61]. The presently used non-EPI DWI method combines a sensitivity of 91.4 % and a positive predictive value of 97.3 % with a negative predictive value of 85 % [62]. Non-EPI DWI thus can prevent unnecessary revision surgery in patients who are suspected of having recurrent or residual disease as CT cannot discriminate cholesteatoma within a soft-tissue mass or partially filled with nonspecific imaging abnormalities [62]. DWI may also replace delayed gadolinium-enhanced T1w sequences [60]. Images from non-EPI sequences or newer EPI techniques such as RESOLVE can even be fused with anatomical images (T1w and T2w) in coronal and/or axial orientation to better localize suspected lesions [63, 64]. This also helps to differentiate e. g. the characteristic T1 hyperintensity of cholesterol granuloma, or asymmetric apex fat, and opacified/infected petrous apex [65].

Conclusion

The diagnostic power of MRI is strongly related to the appropriate selection and interpretation of imaging protocols and sequences based on relevant clinical information. Basic sequences and fat suppression techniques are important tools in the diagnostic workup of inflammation, congenital lesions and tumors including staging. Additional high-resolution sequences are used to evaluate pathologies of the cranial nerves and labyrinth, and to evaluate endolymphatic hydrops in Menière's disease. Vessel and perfusion sequences are used in vascular contact syndromes, vascular malformations and analysis of microvascular parameters of tissue perfusion. Diffusion-weighted imaging is helpful in cholesteatoma imaging, estimation of malignancy, and evaluation of treatment response and post-treatment recurrence in head & neck cancer. Close collaboration with referring physicians and active participation in multidisciplinary conferences, such as tumor, pediatric, and vascular malformation boards seem important to improve knowledge obtained from MRI in the daily routine and to drive further research in this fascinating image modality.

Conflict of Interest

The authors declare that they have no conflict of interest.

References

[1] Lenz M, Greess H, Dobritz M et al. Methods: MRT. European journal of radiology 2000; 33: 178 – 184

[2] Bender B, Widmann G, Riechelmann H et al. Cervicalgia with increased C-reactive protein levels. Der Radiologe 2014; 54: 262 – 264

[3] Hoang JK, Branstetter BFT, Eastwood JD et al. Multiplanar CT and MRI of collections in the retropharyngeal space: is it an abscess? Am J Roentgenol 2011; 196: W426 – W432

[4] Adams A, Mankad K, Offiah C et al. Branchial cleft anomalies: a pictorial review of embryological development and spectrum of imaging findings. Insights Imaging 2016; 7: 69 – 76

[5] Lenz M, Greess H, Baum U et al. Oropharynx, oral cavity, floor of the mouth: CT and MRI. European journal of radiology 2000; 33: 203 – 215

[6] Jeon TY, Kim HJ, Chung SK et al. Sinonasal inverted papilloma: value of convoluted cerebriform pattern on MR imaging. AJNR Am J Neuroradiol 2008; 29: 1556 – 1560

[7] van Gils AP, van den Berg R, Falke TH et al. MR diagnosis of paraganglioma of the head and neck: value of contrast enhancement. Am J Roentgenol 1994; 162: 147 – 153

[8] Moonis G, Cunnane MB, Emerick K et al. Patterns of perineural tumor spread in head and neck cancer. Magn Reson Imaging Clin N Am 2012; 20: 435 – 446

[9] Eisen MD, Yousem DM, Montone KT et al. Use of preoperative MR to predict dural, perineural, and venous sinus invasion of skull base tumors. AJNR Am J Neuroradiol 1996; 17: 1937 – 1945

[10] Ko B, Parvathaneni U, Hudgins PA et al. Do Radiologists Report the TNM Staging in Radiology Reports for Head and Neck Cancers? A National Survey Study. AJNR Am J Neuroradiol 2016; 37: 1504 – 1509

[11] Li C, Yang W, Men Y et al. Magnetic resonance imaging for diagnosis of mandibular involvement from head and neck cancers: a systematic review and meta-analysis. PLoS One 2014; 9: e112267

This document was downloaded for personal use only. Unauthorized distribution is strictly prohibited.

[12] Becker M, Zbaren P, Casselman JW et al. Neoplastic invasion of laryngeal cartilage: reassessment of criteria for diagnosis at MR imaging. Radiology 2008; 249: 551 – 559

[13] Lell M, Baum U, Greess H et al. Head and neck tumors: imaging recurrent tumor and post-therapeutic changes with CT and MRI. European journal of radiology 2000; 33: 239 – 247

[14] King AD, Keung CK, Yu KH et al. T2-weighted MR imaging early after chemoradiotherapy to evaluate treatment response in head and neck squamous cell carcinoma. AJNR Am J Neuroradiol 2013; 34: 1237 – 1241

[15] Schmutzhard J, Widmann G, Abraham I et al. Headache and hypoglossal nerve palsy. Hno 2009; 57: 690 – 692

[16] de Bondt BJ, Stokroos R, Casselman JW et al. Clinical impact of short tau inversion recovery MRI on staging and management in patients with cervical lymph node metastases of head and neck squamous cell carcinomas. Head Neck 2009; 31: 928 – 937

[17] Ma J. Dixon techniques for water and fat imaging. J Magn Reson Imaging 2008; 28: 543 – 558

[18] Vogl T, Bisdas S. Lymph node staging. Top Magn Reson Imaging 2007; 18: 303 – 316

[19] Kimura Y, Sumi M, Sakihama N et al. MR imaging criteria for the prediction of extranodal spread of metastatic cancer in the neck. AJNR Am J Neuroradiol 2008; 29: 1355 – 1359

[20] Sheth S, Branstetter BFT, Escott EJ. Appearance of normal cranial nerves on steady-state free precession MR images. Radiographics 2009; 29: 1045 – 1055

[21] Dubrulle F, Kohler R, Vincent C et al. Differential diagnosis and prognosis of T1-weighted post-gadolinium intralabyrinthine hyperintensities. European radiology 2010; 20: 2628 – 2636

[22] Dubrulle F, Souillard R, Chechin D et al. Diffusion-weighted MR imaging sequence in the detection of postoperative recurrent cholesteatoma. Radiology 2006; 238: 604 – 610

[23] Gurkov R, Pyyko I, Zou J et al. What is Meniere's disease? A contemporary re-evaluation of endolymphatic hydrops. J Neurol 2016; 263: S71 – S81

[24] Naganawa S, Nakashima T. Visualization of endolymphatic hydrops with MR imaging in patients with Meniere's disease and related pathologies: current status of its methods and clinical significance. Jpn J Radiol 2014; 32: 191 – 204

[25] Nakashima T, Naganawa S, Pyykko I et al. Grading of endolymphatic hydrops using magnetic resonance imaging. Acta Otolaryngol Suppl 2009; 560: 5 – 8

[26] Sirikci A, Bayazit Y, Ozer E et al. Magnetic resonance imaging based classification of anatomic relationship between the cochleovestibular nerve and anterior inferior cerebellar artery in patients with non-specific neuro-otologic symptoms. Surg Radiol Anat 2005; 27: 531 – 535

[27] Le Y, Kroeker R, Kipfer HD et al. Development and evaluation of TWIST Dixon for dynamic contrast-enhanced (DCE) MRI with improved acquisition efficiency and fat suppression. J Magn Reson Imaging 2012; 36: 483 – 491

[28] Romano A, Tavanti F, Rossi Espagnet MC et al. The role of time-resolved imaging of contrast kinetics (TRICKS) magnetic resonance angiography (MRA) in the evaluation of head-neck vascular anomalies: a preliminary experience. Dentomaxillofac Radiol 2015; 44: 20140302

[29] Razek AA, Gaballa G, Megahed AS et al. Time resolved imaging of contrast kinetics (TRICKS) MR angiography of arteriovenous malformations of head and neck. European journal of radiology 2013; 82: 1885 – 1891

[30] Higgins LJ, Koshy J, Mitchell SE et al. Time-resolved contrast-enhanced MRA (TWIST) with gadofosveset trisodium in the classification of soft-tissue vascular anomalies in the head and neck in children following updated 2014 ISSVA classification: first report on systematic evaluation of MRI and TWIST in a cohort of 47 children. Clinical radiology 2016; 71: 32 – 39

[31] Yuan J, Chow SK, Yeung DK et al. A five-colour colour-coded mapping method for DCE-MRI analysis of head and neck tumours. Clinical radiology 2012; 67: 216 – 223

[32] Bernstein JM, Homer JJ, West CM. Dynamic contrast-enhanced magnetic resonance imaging biomarkers in head and neck cancer: potential to guide treatment? A systematic review. Oral Oncol 2014; 50: 963 – 970

[33] O'Connor JP, Jackson A, Parker GJ et al. Dynamic contrast-enhanced MRI in clinical trials of antivascular therapies. Nat Rev Clin Oncol 2012; 9: 167 – 177

[34] Chawla S, Kim S, Loevner LA et al. Prediction of disease-free survival in patients with squamous cell carcinomas of the head and neck using dynamic contrast-enhanced MR imaging. AJNR Am J Neuroradiol 2011; 32: 778 – 784

[35] Kim S, Loevner LA, Quon H et al. Prediction of response to chemoradiation therapy in squamous cell carcinomas of the head and neck using dynamic contrast-enhanced MR imaging. AJNR Am J Neuroradiol 2010; 31: 262 – 268

[36] Gaddikeri S, Gaddikeri RS, Tailor T et al. Dynamic Contrast-Enhanced MR Imaging in Head and Neck Cancer: Techniques and Clinical Applications. AJNR Am J Neuroradiol 2016; 37: 588 – 595

[37] Gaddikeri S, Hippe DS, Anzai Y. Dynamic Contrast-Enhanced MRI in the Evaluation of Carotid Space Paraganglioma versus Schwannoma. J Neuroimaging 2016; 26: 618 – 625

[38] Hermans R, Vandecaveye V. Diffusion-weighted MRI in head and neck cancer. Cancer Imaging 2007; 7: 126 – 127

[39] Bammer R. Basic principles of diffusion-weighted imaging. Eur J Radiol 2003; 45: 169 – 184

[40] White ML, Zhang Y, Robinson RA. Evaluating tumors and tumorlike lesions of the nasal cavity, the paranasal sinuses, and the adjacent skull base with diffusion-weighted MRI. J Comput Assist Tomogr 2006; 30: 490 – 495

[41] Schwartz KM, Lane JI, Bolster BD Jr et al The utility of diffusion-weighted imaging for cholesteatoma evaluation. AJNR American journal of neuroradiology 2011; 32: 430 – 436

[42] De Foer B, Vercruysse JP, Bernaerts A et al. Detection of postoperative residual cholesteatoma with non-echo-planar diffusion-weighted magnetic resonance imaging. Otology & neurotology: official publication of the American Otological Society, American Neurotology Society [and] European Academy of Otology and Neurotology 2008; 29: 513 – 517

[43] Forbes KP, Pipe JG, Karis JP et al. Improved image quality and detection of acute cerebral infarction with PROPELLER diffusion-weighted MR imaging. Radiology 2002; 225: 551 – 555

[44] Mas-Estelles F, Mateos-Fernandez M, Carrascosa-Bisquert B et al. Contemporary non-echo-planar diffusion-weighted imaging of middle ear cholesteatomas. Radiographics 2012; 32: 1197 – 1213

[45] Thoeny HC, De Keyzer F, King AD. Diffusion-weighted MR imaging in the head and neck. Radiology 2012; 263: 19 – 32

[46] Yun TJ, Kim JH, Kim KH et al. Head and neck squamous cell carcinoma: differentiation of histologic grade with standard- and high-b-value diffusion-weighted MRI. Head Neck 2013; 35: 626 – 631

[47] Wang J, Takashima S, Takayama F et al. Head and neck lesions: characterization with diffusion-weighted echo-planar MR imaging. Radiology 2001; 220: 621 – 630

[48] Driessen JP, Caldas-Magalhaes J, Janssen LM et al. Diffusion-weighted MR imaging in laryngeal and hypopharyngeal carcinoma: association between apparent diffusion coefficient and histologic findings. Radiology 2014; 272: 456 – 463

[49] de Bondt RB, Hoeberigs MC, Nelemans PJ et al. Diagnostic accuracy and additional value of diffusion-weighted imaging for discrimination of malignant cervical lymph nodes in head and neck squamous cell carcinoma. Neuroradiology 2009; 51: 183 – 192

This document was downloaded for personal use only. Unauthorized distribution is strictly prohibited.

[50] Vandecaveye V, De Keyzer F, Vander Poorten V et al. Head and neck squamous cell carcinoma: value of diffusion-weighted MR imaging for nodal staging. Radiology 2009; 251: 134 – 146

[51] King AD, Chow KK, Yu KH et al. Head and neck squamous cell carcinoma: diagnostic performance of diffusion-weighted MR imaging for the prediction of treatment response. Radiology 2013; 266: 531 – 538

[52] King AD, Mo FK, Yu KH et al. Squamous cell carcinoma of the head and neck: diffusion-weighted MR imaging for prediction and monitoring of treatment response. European radiology 2010; 20: 2213 – 2220

[53] Driessen JP, van Kempen PM, van der Heijden GJ et al. Diffusion-weighted imaging in head and neck squamous cell carcinomas: a systematic review. Head Neck 2015; 37: 440 – 448

[54] Sasaki M, Yamada K, Watanabe Y et al. Variability in absolute apparent diffusion coefficient values across different platforms may be substantial: a multivendor, multi-institutional comparison study. Radiology 2008; 249: 624 – 630

[55] Payne KF, Haq J, Brown J et al. The role of diffusion-weighted magnetic resonance imaging in the diagnosis, lymph node staging and assessment of treatment response of head and neck cancer. Int J Oral Maxillofac Surg 2015; 44: 1 – 7

[56] Kolff-Gart AS, Pouwels PJ, Noij DP et al. Diffusion-weighted imaging of the head and neck in healthy subjects: reproducibility of ADC values in different MRI systems and repeat sessions. AJNR Am J Neuroradiol 2015; 36: 384 – 390

[57] Chen S, Ikawa F, Kurisu K et al. Quantitative MR evaluation of intracranial epidermoid tumors by fast fluid-attenuated inversion recovery imaging and echo-planar diffusion-weighted imaging. AJNR American journal of neuroradiology 2001; 22: 1089 – 1096

[58] Bergui M, Zhong J, Bradac GB et al. Diffusion-weighted images of intracranial cyst-like lesions. Neuroradiology 2001; 43: 824 – 829

[59] Aikele P, Kittner T, Offergeld C et al. Diffusion-weighted MR imaging of cholesteatoma in pediatric and adult patients who have undergone middle ear surgery. Am J Roentgenol 2003; 181: 261 – 265

[60] De Foer B, Vercruysse JP, Bernaerts A et al. Middle ear cholesteatoma: non-echo-planar diffusion-weighted MR imaging versus delayed gadolinium-enhanced T1-weighted MR imaging–value in detection. Radiology 2010; 255: 866 – 872

[61] Vercruysse JP, De Foer B, Pouillon M et al. The value of diffusion-weighted MR imaging in the diagnosis of primary acquired and residual cholesteatoma: a surgical verified study of 100 patients. European radiology 2006; 16: 1461 – 1467

[62] Jindal M, Riskalla A, Jiang D et al. A systematic review of diffusion-weighted magnetic resonance imaging in the assessment of postoperative cholesteatoma. Otology & neurotology: official publication of the American Otological Society, American Neurotology Society [and] European Academy of Otology and Neurotology 2011; 32: 1243 – 1249

[63] Watanabe T, Ito T, Furukawa T et al. The efficacy of color mapped fusion images in the diagnosis and treatment of cholesteatoma using transcanal endoscopic ear surgery. Otology & neurotology: official publication of the American Otological Society, American Neurotology Society [and] European Academy of Otology and Neurotology 2015; 36: 763 – 768

[64] Kanoto M, Sugai Y, Hosoya T et al. Detectability and anatomical correlation of middle ear cholesteatoma using fused thin slice non-echo planar imaging diffusion-weighted image and magnetic resonance cisternography (FTS-nEPID). Magn Reson Imaging 2015; 33: 1253 – 1257

[65] De Foer B, Vercruysse JP, Spaepen M et al. Diffusion-weighted magnetic resonance imaging of the temporal bone. Neuroradiology 2010; 52: 785 – 807

This document was downloaded for personal use only. Unauthorized distribution is strictly prohibited.